DOE/ER/05002-15
COO-5002-15

COMPUTER SIMULATION STUDY OF THE STRUCTURE OF VACANCIES IN GRAIN BOUNDARIES

A. Brokman,* P. D. Bristowe and R. W. Balluffi

Department of Materials Science and Engineering
Massachusetts Institute of Technology
Cambridge, Massachusetts 02139

* Also at Bergman School of Applied Science, Hebrew University of Jerusalem, Israel

January 1981

Massachusetts Institute of Technology
Cambridge, Massachusetts 02139

Prepared for
U.S. Department of Energy
under Contract DE-AS02-78ER05002.A001

DISCLAIMER

ABSTRACT

The structure of vacancies in grain boundaries has been investigated by computer molecular statics employing pairwise potentials. In order to gain an impression of the vacancy structures which may occur generally, a number of variables was investigated including: metal type, boundary type, degree of lattice coincidence and choice of boundary site. In all cases the vacancies remained as distinguishable point defects in the relatively irregular boundary structures. However, it was found that the vacancy often induced relatively large atomic displacements in the core of the boundary. These displacements often occurred only in the direct vicinity of the vacancy, but in certain cases they were widely distributed in the boundary, sometimes at surprisingly large distances. In certain cases the displacements included a large inward relaxation of one, or more, of the atoms neighboring the vacancy, and the initial vacant site became effectively "split". These results were classified and discussed in relation to the variables listed above. Several binding energies to the boundary were also calculated. Finally, the relevance of the results to the mechanism of boundary self-diffusion was discussed.

1. INTRODUCTION

It has often been assumed (or suggested) [1-3] that vacancies exist in high angle grain boundaries as bona fide point defects, i.e., as distinguishable missing atoms in the structure, and that they can diffuse in the boundary via the adjoining lattice. It has also been concluded that the relatively rapid atomic diffusion observed in grain boundaries [1,2] most probably occurs by the exchange of atoms with such vacancies in thermal equilibrium. Despite the importance of these phenomena relatively little effort has been made in past years to establish a satisfactory understanding of the structure and properties of vacancies in grain boundaries. Several authors [4,5,6] have modeled grain boundary vacancies using the computer simulation approach. However, their work did not focus on the relaxed structure of the vacancy, and, moreover, they considered only a small angle boundary or a coherent twin, both of which are of limited interest.

Most recently, we have presented a preliminary account [7] of attempts to study the structure of vacancies in several grain boundaries using computer simulation employing the method of molecular statics and also simulation employing bubble raft and dynamic hard sphere models. In all cases, and in all models, the vacancies indeed existed as distinguishable point defects even though they may have been considerably relaxed in certain cases. Also, in all cases the atomic relaxations around the vacancies in the grain boundaries were greater than in the corresponding perfect lattice. This result was attributed to the more irregular and lower symmetry structures present in the cores of the boundaries which allowed a variety of short-range order environments to exist. Also, at about the same time, Hahn and Gleiter [8,9] obtained some additional results regarding the relaxation of vacancies in grain boundaries, using a static

computer simulation model employing a Morse potential, which are similar in some respects to those reported in [7].

In the present paper we describe the results of a considerably more extensive study of vacancies in grain boundaries using the computer simulation method. As pointed out previously [7], there is a number of inherent difficulties in carrying out such a program. Firstly, grain boundaries possess irregular atomic structures making the structure of a vacancy in a grain boundary somewhat difficult to define and describe. Secondly, the vacancy structure varies with its position in the boundary. Thirdly, an infinite number of different grain boundary structures exists depending upon the nine degrees of freedom of the boundary, i.e., crystal misorientation, orientation of the boundary plane, etc. Fourthly, the results depend upon the crystal structure of the adjoining grains and on the specific metal which is involved. Consequently, it is necessary to study vacancy structures in boundaries over a wide range of conditions in order to obtain an overall impression of the structures which may occur generally. We have attempted to cope with this situation in the present work by calculating vacancy structures over the rather wide range of variables shown schematically in Fig. 1.

2. COMPUTATIONAL PROCEDURES

To determine the relaxed formation energies and displacement fields of the defects considered in this paper the method of computer molecular statics has been employed. Many of the advantages and disadvantages of using this technique have been examined previously [10,11], and only one particular aspect, namely, the effect of ignoring temperature and entropy, will be mentioned further in this work (see Section 4). Basically, the method involves the creation of a model bicrystal in the appropriate orien-

tation consisting of an assembly of atoms which interact via an assumed pairwise central force interatomic potential. The equilibrium grain boundary configuration is then found by minimizing the total potential energy of the system with respect to the atomic positions. The periodicity of the Coincidence Site Lattice (CSL) is usually utilized to create a computational cell of minimum dimensions which does not constrain the relaxation.

A vacancy is then introduced in the relaxed and equilibrated boundary by simply removing an atom from a preselected site in the boundary, and the structure is again relaxed. In this operation the periodicity of the structure is lost, and a much larger computational cell is required. Thus, when simulating the interaction of a vacancy with a grain boundary a model containing a multiple number of unit CSL cells is used primarily to reduce the influence of the borders on the relaxation. Also, since it is still desirable to impose periodic border conditions in the plane of the boundary, the model dimensions should also be sufficiently large to minimize the mutual interaction between vacancies in the infinite vacancy array that is effectively being simulated. In all of the models used in the present calculations, with the possible exception of cases where the vacancy relaxations in the boundary were exceptionally large, the interfering effect of borders, surfaces and neighboring cells is thought to be minimal.

Four semi-empirical interatomic potentials were used in the calculations, two representing bcc iron and tungsten [12] and two representing fcc copper and nickel [13]. Also, a Lennard-Jones potential with parameters appropriate to krypton was used (see Fig. 2). The semi-empirical

potentials consisted of cubic splines fitted to various bulk properties of the metals concerned, and in the case of iron the potential was matched to the elastic constants so as to obey the Cauchy relation. Thus, the iron potential was an equilibrium potential, whereas the others were non-equilibrium and predicted non-zero values for the Cauchy pressure.

The purpose of the present calculations was to determine the spatial relaxation field around an isolated stationary vacancy in a grain boundary and also compute the vacancy formation (or binding) energy. No attempt was made to determine the migration energy of the vacancies in the grain boundary by moving them along a preselected path. Although such calculations are possible using a static procedure (see, e.g., [5,14]), it is undoubtedly more appropriate to employ molecular dynamics in such cases. It should be emphasized that the removal of atoms created genuine extrinsic point defects and not the so-called "structural vacancies" which in some studies [15] have formed part of the procedure for obtaining the equilibrium boundary structure.

The exact calculation of the formation energy E_B^F (or binding energy E_B^B) of a vacancy in the boundary requires a knowledge of its formation volume Ω_B^F in the boundary. Thus, in a manner analogous to the calculation of the formation energy of a vacancy in a single crystal [16], the grain boundary vacancy formation energy is given by

$$E_B^F = E_B^{PP} + p\Omega_B^F \qquad (1)$$

where E_B^{PP} is a grain boundary pair potential term, and p is the Cauchy pressure. The binding energy of the vacancy to the boundary is then given

by

$$E_B^B = E_B^F - E_L^F$$
$$= E_B^{PP} - E_L^{PP} + p\Omega_B^F - p\Omega_L^F \qquad (2)$$

where E_L^F, E_L^{PP} and Ω_L^F are the formation energy, pair potential term and formation volume of the vacancy in the single crystal, respectively. The value of Ω_L^F has been calculated most recently [16,17] by evaluating the defect strength tensor which is related to the forces and positions of atoms remote from the defect near the borders of the computational cell. This method would be difficult to apply in the case of a grain boundary vacancy, especially one that is split as described below in Section 3. Therefore, two simplifying cases are considered here. Clearly, if an equilibrium potential is used in which the Cauchy pressure is zero, $p\Omega_B^F = p\Omega_L^F = 0$, and it unnecessary to compute the formation volumes. Also, if it is assumed when using a non-equilibrium potential that $\Omega_B^F \simeq \Omega_L^F$, which is fairly accurate for a non-split grain boundary vacancy, then $p\Omega_B^F \simeq p\Omega_L^F$, and, again, only the pair potential terms contribute to the formation and binding energies. When the vacancy is split in the boundary such an approximation is less valid, and, therefore, only crude estimates of E_B^F and E_B^B may be made.

Finally, it should be pointed out that these energy calculations may be strongly dependent on various basic assumptions involved in constructing the interatomic potentials. In particular, it has recently been argued [18] that three-body forces are necessary to describe correctly the vacancy formation energy in a metal such as aluminum. However, the effect of these forces on the vacancy formation energy in more complex systems, such as the noble and transition metals, although unknown, is thought to be less important.

3. RESULTS

We now present a selection of results which is thought to be typical of the range of effects that can occur. As indicated in Fig. 1, results for vacancies in two types (pure tilt and twist) of boundaries with differing degrees of coincidence (Σ=5, 13, and 25) are given. Boundary configurations in both bcc and fcc lattice structures are considered in a number of metals, and in the case of tilt boundaries the effect of boundary asymmetry is also investigated. Finally, vacancy structures in different sites in several boundaries are shown.

For simplicity, the results for the relaxed structures and the binding energies are described separately in Sections 3.1 and 3.2. Finally (in Section 4), the results are discussed together and related to the variables described above.

3.1 Relaxed Structures

In many cases it was found that the introduction of a vacancy induced relatively large atomic displacements in the core of the grain boundary.* These displacements often occurred only in the direct vicinity of the vacancy, but in certain cases they were widely distributed in the boundary, sometimes at surprisingly large distances. Also, in certain cases the displacement included a large inward relaxation of one, or more, of the neighboring atoms surrounding the vacant site. In such cases the initial vacant site became effectively "split". In the following discussion we therefore pay particular attention to the following questions. Did the

---

* It is emphasized that these displacements were very much larger than the usual elastic displacements expected of a point center of dilation in a perfect lattice and are a result of the fact that atoms in the relatively disordered structure in the boundary core may be more easily displaced than perfect lattice atoms.

vacancy induce large atomic displacements in the grain boundary? Were the displacements widely distributed or were they localized very near the vacancy? Did the displacements split the vacancy? The following criteria were adopted in order to classify objectively the answers to these questions:

(i) a "large" displacement is one which is larger than 20% of the nearest-neighbor distance in the perfect lattice;

(ii) the displacements are "widely distributed" if large displacements are induced at distances beyond the atoms neighboring the vacant site;

(iii) a vacancy is "split" if a neighboring atom is displaced into the vacancy site by a "large" displacement (i.e., one larger than 20% of the nearest-neighbor distance).

The results for all of the vacancies examined are summarized in Table 1.

Σ=5 (36.9°) [100] tilt boundaries: Figures 3(a,b) show the relaxed displacement field before and after the insertion of a vacancy (at the encircled atomic site labeled 1) into a bcc Σ=5 (36.9°) [100] tilt boundary with the boundary plane parallel to $(310)_{1,2}$. The empirical potential representing iron was used, and the atomic relaxations caused by the removal of an atom are shown as vector displacements projected onto the plane of the paper which is an edge-on view down the tilt axis. It may be seen that the vacancy induced boundary displacements are relatively small and that the vacancy remains non-split as indicated in Table 1. Figures 3(c,d) show the corresponding structures using the potential representing tungsten. In this case one neighboring atom experiences a large displacement into the vacancy. Therefore, one large displacement occurs, the displacements are not widely distributed, and the vacancy is split.

In order to investigate the effect of changing the vacancy site in a tilt boundary of given structure a vacancy was introduced into the atomic site labeled 2 in Fig. 3(a) which is very close to an O-Lattice point [19]* in the boundary which is shown by the X. Again, the boundary displacements are small, and the vacancy remains non-split.

Figures 4(a,b) show the relaxed displacement field produced by the insertion of a vacancy into a fcc Σ=5 (36.9°) [100] tilt boundary with the boundary plane parallel to $(310)_{1,2}$. The empirical potential representing nickel was used in this case, and the same illustration conventions are used as in Fig. 3. Figures 4(c,d) show the corresponding structures using the potential for copper. As in the results for the tilt boundary in bcc iron, the displacements in the nickel boundary are small and the vacancy remains non-split. However, in the copper boundary one large inward displacement of a neighboring atom occurs causing the vacancy to become split.

The calculations for the fcc tilt boundary were repeated using the Lennard-Jones potential for krypton, and it was found that the vacancy induced boundary displacements were exceedingly small. In fact, on the scale of the figures presented here, the displacement vectors were not visible.

Figures 5(a,b) show the relaxed displacement field before and after the insertion of a vacancy into a bcc Σ=5 (36.9°) [100] asymmetric boundary where the average boundary plane is parallel to $(430)_1$. The potential representing tungsten was used in this example, and it is seen that all displacements are small. A comparison of Figs. 5(a,b) with Figs. 3(c,d) shows that the introduction of asymmetry does not greatly affect the nature of the vacancy displacement field, since the only significant difference is

* All O-Lattices employed in the present paper correspond to rotational transformations around [100] which relate nearest-neighboring atoms of Lattices 1 and 2.

the existence of one displacement of an atom neighboring the vacancy in the latter case which is barely in the "large" category. A vacancy in the same type of asymmetric tilt boundary in bcc iron was also examined, and all displacements were found to be small. This is the same result as that obtained for the symmetric boundary [Figs. 3(a,b)] in agreement with the above conclusion. The reason for this behavior is most likely that the equilibrium structure of the asymmetric boundary actually consists of segments (or facets) which possess structures corresponding to symmetric boundaries of the same coincidence system. This local atomistic faceting of asymmetric boundaries is thought to be quite general [20]. Since the local vacancy environments are similar in both the symmetric and non-symmetric cases, we may expect generally similar vacancy induced displacements as observed.

Σ=5 (36.9°) [100] twist boundaries: Figures 6(a-d) show the relaxed displacement field before and after the insertion of a vacancy (at the encircled atomic site) into a bcc Σ=5 (36.9°) [100] twist boundary using the potential representing iron. Figures 6(a,b) give the plan and edge-on views of the equilibrium boundary structure without the vacancy, and Figs. 6(c,d) show the atomic relaxations, represented by vector displacements projected on the plane of the paper, after the removal of the atom. It should be noted that the plan view, which is a view down the [100] twist axis, contains nine Σ=5 CLS unit cells and that only four (100) planes (two above and below the twist boundary) are included for clarity. The vector displacements shown in Figs. 6(c,d) illustrate that the displacements are small and that the vacancy is non-split.

Figures 7(a-d) show the corresponding structures using the tungsten

potential. This time the atomic displacements caused by the presence of the vacancy are large and spread over several CSL unit cells. In addition, a significant inward relaxation of atoms neighboring the vacant site has occurred causing the vacancy to become split. This figure, which contrasts sharply with Fig. 6, is an example of a vacancy which is split and has also induced large and widely distributed displacements.

Figures 8(a-d) show the relaxed displacement field before and after the insertion of a vacancy into a fcc Σ=5 (36.9°) [100] twist boundary using the copper potential. The illustration conventions are the same as before, and it is seen that the equilibrium structure of the boundary before the removal of the atom involves an in-plane translation of Lattice 1 with respect to Lattice 2 away from the CSL position [Fig. 8(a)]. Upon relaxation of the boundary vacancy, large displacements occur in the general vicinity of the defect but they are not as extensive as in the case of tungsten. Also, the vacancy is split. Quite a different result was obtained when the nickel potential was employed with this boundary [Figs. 9(a-d)]. Once more the boundary structure involves an in-plane translation, but, upon introducing a vacancy, only one neighboring atom is essentially involved in the relaxation [shown by the large arrow in Fig. 9(d)]. The vacancy splits in order to share two adjacent atomic sites, and an atom sits in the boundary plane midway between Lattices 1 and 2. Thus, this defect induces a large displacement which is localized and causes it to be split in a manner similar to the vacancy described earlier in connection with the copper tilt boundary in Fig. 4(c,d).

In order to investigate the effect of changing the vacancy site in a twist boundary a vacancy was introduced in an O-Lattice site in a

Σ=5 twist boundary in copper under conditions where no in-plane translation of Lattice 1 with respect to Lattice 2 was allowed [see Fig. 10(a)]. This condition preserved occupied O-Lattice sites while making the boundary slightly metastable to the presumably equilibrium structure possessing the in-plane translation shown previously in Fig. 8(a). The structure is shown in Figs. 10(c,d), and it is seen that the vacancy in this site is non-split rather than split [as in Figs. 8(c,d)] and its displacement field is localized. It is interesting to note that all of the small displacements of the atoms neighboring the vacancy are tangential with respect to the center of the vacant site (taken as a center of rotation), and, hence, do not tend to split the vacant site. Furthermore, the introduction of the vacancy induced small displacements elsewhere in the boundary which were mainly tangential to other O-Lattice points in the boundary [Fig. 10(c)]. The structure of an O-Lattice vacant site in another boundary was calculated for the case of the Σ=5 twist boundary in tungsten shown previously in Fig. 7(a). The vacancy in this case [Figs. 11(a,b)] has again induced large displacements which are widely distributed in the boundary. However, the displacements are mainly tangential around the O-Lattice points, and the vacancy remains non-split. The results are generally similar to those obtained for copper except that the displacements are considerably larger and more widely distributed. We note that the structure in Figs. 11(a,b) was not completely equilibrated in the computer due to the long computational time required. However, this feature of the calculation should not have affected the qualitative aspects of the above results.

When the Lennard-Jones potential for krypton was employed to relax the Σ=5 twist boundary the atomic displacements were all very small, and

the vacancy in a non O-Lattice site remained non-split, as was the case with the tilt boundary.

Σ=13 (22.6°) [100] twist boundary: A vacancy was introduced at an O-Lattice site in a Σ=13 twist boundary using the potential for copper, and all displacements were found to be small. Again, the observable displacements were mainly tangential around O-Lattice points, and the displacement field was generally similar in that respect to the one shown in Fig. 10(c,d) for the Σ=5 twist boundary.

Σ=25 (16.3°) [100] tilt boundaries: Figures 12(a,b) show the relaxed displacement field before and after the insertion of a vacancy (at the encircled atomic site) into a bcc Σ=25 (16.3°) [100] tilt boundary with the boundary plane parallel to $(710)_{1,2}$. The potential representing iron was used, and, as before, edge-on views are given with the atomic relaxations due to the vacancy being represented by vector displacements projected on the plane of the paper. As with the Σ=5 tilt boundary, all relaxations are seen to be small, and the vacancy is therefore non-split.

Σ=25 (16.3°) [100] twist boundaries: Figures 13(a-d) show the relaxed displacement field before and after the insertion of a vacancy into a fcc Σ=25 (16.3°) [100] twist boundary using the copper potential. Using the same illustration conventions, it is seen that only one CSL unit cell has been employed, and that the equilibrium boundary structure does not involve an in-plane translation (these translations become less important as Σ increases for twist boundaries). The vector displacement diagrams

show that the vacancy has induced large displacements which are widely distributed but that it remains non-split. The vacancy shown is in a non O-Lattice site (shown by the X). In this case the displacements, which are largely tangential around the O-Lattice site acting as a center, do not split the vacancy but produce an extensive displacement field. It may also be seen that most of the displacements are confined to the two planes directly adjacent to the boundary. A similar effect occurred when using the potential representing nickel with this boundary, and further discussion of this pattern of relaxation is given in Section 4.

3.2 Binding Energies

Following the procedure prescribed in Section 2 the formation and binding energies of the vacancies in the boundaries were calculated. As noted in that section, the calculation could be done "exactly" only for cases where the equilibrium potential for iron was employed. However, even here the calculation should be considered approximate, since the potential has been constructed erroneously from elastic constants that satisfy the Cauchy relation. In addition, the neglect of long-range oscillations and the assumption of two-body forces may also affect the calculations [18]. In the calculations using the other potentials, except the Lennard-Jones one, the assumption that $\Omega_B^F \simeq \Omega_L^F$ has been made which will lead to inaccuracies when the vacancy is split and has induced widely distributed displacements. The results for the binding energy of a vacancy to the various boundaries considered in detail here are given in Table 1. It is seen that a considerable range of binding energies is found which is not surprising in view of the approximations which have been used. The

most reliable values, which are those for the vacancies in iron, indicate an attractive binding energy of ≃ 0.5 eV for non O-Lattice sites in this metal. Further aspects of these results are discussed below.

4. DISCUSSION AND CONCLUSIONS

The more extensive results described in the present paper (summarized in Table 1) confirm our earlier conclusion [7] that vacancies generally remain in grain boundaries as distinguishable point defects. However, their structures may vary considerably (Table 1) depending upon the variables listed in Fig. 1. Several trends were observed which may be summarized as follows:

(i) The vacancy induced boundary displacements in all of the tilt boundaries were localized. Also, the displacements were small in all boundaries with the exception of the Σ=5(310) boundaries in copper and tungsten where the vacancy is split.

(ii) The vacancies in the non O-Lattice sites in twist boundaries tended to split and induce more widely distributed displacements as the "hardness" of the interatomic potential increased. An approximate measure of the hardness of the potential is the space derivative of the interatomic potential at nearest-neighbor and second nearest-neighbor positions in the perfect lattice expressed as a force (see Table 1). Since these atom-atom distances appear frequently in perfect grain boundaries, the "hardness" defined in this way is a crude measure of the ability of the boundary to accommodate local distortion.

(iii) The vacancies in the O-Lattice sites in the twist boundaries were always non-split even though their displacements may have been large and widely distributed.

Observation (i) seems related to the fact that local mirror symmetry was preserved to a large extent in all of the tilt boundaries investigated. This was the case even when small translations from the CSL position were present and when the boundaries were asymmetric. In the latter case, as described earlier, the boundaries were found to undergo atomistic faceting in which the boundary breaks up into small facets each corresponding to a symmetric tilt boundary segment [20]. The immediate environment for a vacancy therefore consists of a symmetric boundary element possessing approximate local mirror symmetry. The tendency of the displacement field to remain localized may then be understood in a general qualitative way on the basis of the higher degree of local symmetry and therefore "order" in these boundaries.

Observation (ii) may be explained on the basis of the effect of the hardness of the potential on the ability of the boundary to accommodate local distortion. With a hard potential, such as for tungsten, the atoms act approximately as hard spheres and are therefore unable to "absorb" distortions locally. The rearrangements associated with the introduction of a vacancy into the boundary therefore tend to propagate (sometimes over relatively large distances), and the vacancy tends to become split and to induce widely distributed displacements. On the other hand, with a softer potential as in krypton, any rearrangements can be accommodated locally by the softer atoms and the vacancy remains localized and non-split.

Observation (iii) must be related to the high degree of symmetry around O-Lattice points in [100] twist boundaries and the general form

of the displacement fields present in such boundaries. In this respect it is recalled that an occupied O-Lattice point is also a CSL point and that atoms on CSL points are "correctly" located with respect to both adjoining lattices. Brokman and Balluffi [22] have recently demonstrated that perfect [100] twist and tilt boundaries exhibit characteristic primary relaxations in each patch of boundary centered on an O-Lattice element. In these relaxations each O-Lattice point acts as a center of rotation where the atoms of Lattices 1 and 2 in its vicinity relax in a tangential direction so as to cause a local reduction in the crystal misorientation (i.e., tilt or twist rotation) to cause better lattice matching across the boundary. There is therefore no (or very little) tendency for atoms very near O-Lattice sites to change their positions due to primary relaxations in the perfect boundary. It is therefore not surprising that a vacancy on an O-Lattice site remains non-split. However, the introduction of a vacancy at either an O-Lattice or a non O-Lattice site may induce relaxations elsewhere in the boundary which tend to either increase or decrease the tangential relaxations described above [see Figs. 7(a), 10(c), 11(a), and 13(c)], and the displacement field associated with the vacancy tends to become widely distributed.

No significant information about the effect of the degree of coincidence (Σ) could be gleaned from the present results. Large displacements were induced in both Σ=5 and 25 twist boundaries in copper and nickel while, on the other hand, the vacancies were split with Σ=5 and not with Σ=25. However, this was probably a result of the choice of sites, since the vacancies in the Σ=25 boundaries were very close to O-Lattice points as seen in Fig. 13. In these boundaries the primary relaxation around the O-Lattice point produces a local patch of boundary centered on the O-Lattice

point which has a structure approaching that of the perfect lattice. (We note that this structure approximates the structure of lower angle [100] twist boundaries where these patches are better defined, and the structure consists of a grid of discrete lattice screw dislocations running between the patches of perfect lattice [21]). Since the vacancies are located in these relatively perfect patches, it is not surprising that they are non-split while at the same time capable of inducing displacements elsewhere in the inhomogeneous boundary.

The binding energies which were calculated are listed in Table 1 and show that the binding energies at, or very near, O-Lattice sites are relatively small. (Two of the energies are actually small and positive, i.e., slightly repulsive. However, this aspect of these results should probably not be taken seriously in view of the expected accuracy of the calculations.) Also, the vacancy in the highly relaxed patch of nearly perfect lattice structure which is associated with the O-Lattice point in the Σ=25 twist boundary in copper possesses a small binding energy. All of these vacancies are non-split, and the relatively low binding energies for these defects seems consistent with this result. Evidently, the relaxations at larger distances which were occasionally induced by these defects caused only small changes in the energy.

We note that the most reliable binding energy calculations, i.e., those for iron, indicate attractive binding energies at non O-Lattice sites which are $\simeq$ 0.5 eV. These correspond to vacancy formation energies in the grain boundary at these sites which are $\simeq$ 0.6 that of the formation energy in the lattice. These results are not inconsistent with a mechanism for fast grain boundary self-diffusion which involves the exchange of atoms

with grain boundary vacancies present in thermal equilibrium as discussed elsewhere [1-3]. The present results indicate that a variety of different types of vacancy jumps between different types of sites will exist as has been postulated elsewhere [1,2,23,24]. Grain boundary diffusion by this mechanism should therefore consist of a spectrum of thermally activated jumping processes. Many of these jumps should be relatively easy, particularly for split vacancies where atomic shuffles involving relatively small energy barriers to thermal activation would be required.

Further calculations over an even wider range of boundary types and sites than covered in the present work would have been interesting in order to establish more firmly some of the trends suggested by the results achieved to date. However, limitations on available computer time made such an effort impractical. However, further studies of point defects in boundaries are in progress. We are currently making a comparable study of the structure and energy of self-interstial atoms in grain boundaries in order to investigate the properties of these defects and to evaluate their possible role in the grain boundary self-diffusion process. In addition, we are studying the structure of boundaries and their vacancy point defects at finite temperatures using the method of molecular dynamics in collaboration with T. Kwok and S. Yip at M.I.T. In this work we are searching for conceivable changes in structure due to temperature (entropy) effects as the bicrystal is heated to elevated temperatures [25] and are also observing directly the migration of grain boundary vacancies and the relationship of this to grain boundary self-diffusion.

ACKNOWLEDGMENTS

Support was provided by the U.S. Department of Energy (Contract DE-AS02-78ER05002.A001) for A.B. and R.W.B., and by the National Science Foundation (Grant DMR 78-12804) for P.D.B. and R.W.B. The authors also wish to acknowledge the use of computer codes developed at AERE Harwell and at the University of Surrey.

Table 1. Data for Grain Boundary Vacancies.

		Force (eV Å^{-1})					Vacancy Induced Boundary Displacements		
		Nearest-Neighbor	Second Nearest-Neighbor	Lattice Vacancy Formation Energy (eV)	Boundary Type	Boundary Vacancy Binding Energy (eV)	Large?	Widely Distributed?	Vacancy Split?
FCC	Kr	-0.003	0.003	0.1	tilt, Σ5(310)	–	no	no	no
					twist, Σ5	0.3	no	no	no
	Cu	-0.359	0.018	1.4	tilt, Σ5(310)	-1.4[d]	yes	no	yes
					twist, Σ5	-0.5	yes	yes	yes
					twist, Σ5[a]	0.3	no	no	no
					twist, Σ13[a]	0.2	no	no	no
					twist, Σ25[c]	0.0	yes	yes	no
	Ni	-0.382	0.321	1.4	tilt, Σ5(310)	-0.7	no	no	no
					twist, Σ5	-0.7	yes	no	yes
					twist, Σ25[c]	–	yes	yes	no
BCC	Fe	-0.305	0.352	1.4	tilt, Σ5(310)	-0.4	no	no	no
					tilt, Σ5(310)[b]	0.0	no	no	no
					tilt, Σ5(430)	–	no	no	no
					tilt ,Σ25(710)	-0.6	no	no	no
					twist, Σ5	-0.6	no	no	no
	W	-1.155	0.695	5.5	tilt, Σ5(310)	–	yes	no	yes
					tilt, Σ5(430)	–	no	no	no
					twist, Σ5	–	yes	yes	yes
					twist, Σ5[a]	–	yes	yes	no

[a] Vacancy on O-Lattice site (all other vacancies listed in Table are on non O-Lattice sites).

[b] Very close to C-Lattice site [on site labeled 2, Fig. 3(a)].

[c] Vacancy in patch of almost single crystal centered on O-Lattice point.

[d] Binding energy particularly uncertain (see Section 2 in text).

REFERENCES

1. N. A. Gjostein, in Diffusion, p. 241, American Society for Metals, Metals Park (1973).

2. N. L. Peterson, in Grain Boundary Structure and Kinetics, p. 209, ASM, Metals Park (1980).

3. R. W. Balluffi, in Grain Boundary Structure and Kinetics, p. 297, ASM, Metals Park (1980).

4. K. W. Ingle, P. D. Bristowe and A. G. Crocker, Phil. Mag. 33, 663 (1976).

5. B. A. Faridi and A. G. Crocker, Phil. Mag. A41, 137 (1980).

6. R. E. Dahl, J. R. Beeler and R. D. Bourquin, in Interatomic Potentials and Simulation of Lattice Defects, p. 673, Plenum Press, New York (1972).

7. P. D. Bristowe, A. Brokman, F. Spaepen and R. W. Balluffi, Scripta Met. 14, 943 (1980).

8. W. Hahn, Diploma Thesis, University of Saarbrücken (1980).

9. W. Hahn and H. Gleiter, to be published.

10. P. C. Gehlen, J. R. Beeler and R. I. Jaffee (editors), Interatomic Potentials and Simulation of Lattice Defects, Plenum Press, New York (1972).

11. R. J. Arsenault, J. R. Beeler and J. A. Simmons (editors), Computer Simulation for Materials Applications, Nucl. Metall. 20, Parts 1 and 2 (1976).

12. P. D. Bristowe and A. G. Crocker, Phil. Mag. 31, 503 (1975).

13. P. D. Bristowe and A. G. Crocker, Phil. Mag. A38, 487 (1978).

14. K. W. Ingle and A. G. Crocker, Phil. Mag. A37, 297 (1978).

15. G. A. Bruggeman, G. H. Bishop, J. A. Cox and R. J. Harrison, in Computer Simulation for Materials Applications, Nucl. Metall. 20, 450 (1976).

16. A. G. Crocker, M. Doneghan and K. W. Ingle, Phil. Mag. A41, 21 (1980).

17. H. R. Schober, J. Phys. F. 7, 1127 (1977).

18. R. Taylor, in Interatomic Potentials and Computer Simulation of Defects in Metals, TMS-AIME, in press (1980).

19. W. Bollmann, Crystal Defects and Crystalline Interfaces, p. 148, Springer-Verlag, New York (1970).

20. A. Brokman, P. D. Bristowe and R. W. Balluffi, Scripta Met., in press (1981).

21. T. Schober and R. W. Balluffi, Phil. Mag. 21, 109 (1970).

22. A. Brokman and R. W. Balluffi, submitted for publication (1981).

23. P. Benoist and G. Martin, J. de Physique C4, 213 (1975).

24. V. Coste, P. Benoist and G. Martin, 19th Colloque de Métallurgie, p. 507, C.E.N. Saclay (1976).

25. R. W. Balluffi, in Interfacial Segregation (edited by W. C. Johnson and J. M. Blakely) p. 193, ASM, Metals Park (1979).

FIGURE CAPTIONS

Fig. 1 A schematic diagram showing the range of variables studied in the calculation of the boundary vacancy structures.

Fig. 2 The interatomic potential $\phi(r)$ for copper and nickel (see Ref. 13) and for iron and tungsten (see Ref. 12) which were used in the calculations. Also used was a Lennard-Jones "6-12" potential with parameters appropriate to krypton. The vertical strokes on the curves indicate the location of the first and second nearest-neighbor distances, and a is the lattice parameter.

Fig. 3 Displacement fields around a vacancy in a [100] bcc symmetric tilt boundary (Σ=5, θ = 36.87°, boundary plane parallel to $(310)_{1,2}$).
(a) and (c) Edge-on views of relaxed structure in iron and tungsten, respectively, before insertion of vacancy at encircled atom. O-Lattice point at X.
(b) and (d) Corresponding edge-on views of atomic relaxations around the vacancy. Each atomic relaxation is represented by a vector displacement projected on the plane of the paper.

Fig. 4 Displacement fields around a vacancy in a [100] fcc symmetric tilt boundary (Σ=5, θ =36.87°, boundary plane parallel to $(310)_{1,2}$).
(a) and (c) Edge-on views of relaxed structure in nickel and copper, respectively, before insertion of vacancy at encircled atom. (b) and (d) Corresponding edge-on views of atomic relaxations around the vacancy. Each atomic relaxation is represented by a vector displacement projected on the plane of the paper.

Fig. 5 Displacement field around a vacancy in a [100] bcc asymmetric tilt boundary in tungsten (Σ=5, θ = 36.87°, boundary plane parallel to

$(430)_1$). (a) Edge-on view of relaxed structure before insertion of vacancy at encircled atom. (b) Edge-on view of atomic relaxations around the vacancy. Each atomic relaxation is represented by a vector displacement projected on the plane of the paper.

Fig. 6 Displacement field around a vacancy in a [100] twist boundary (Σ=5, θ = 36.87°) in bcc iron. (a) and (b) Plan and edge-on views of relaxed structure before insertion of vacancy at encircled atom. (c) and (d) Plan and edge-on views of atomic relaxations around the vacancy. Each atomic relaxation is represented by a vector displacement projected on the plane of the paper.

Fig. 7 Displacement field around a vacancy in a [100] twist boundary (Σ=5, θ = 36.87°) in bcc tungsten. (a) and (b) Plan and edge-on views of relaxed structure before insertion of vacancy at encircled atom. (c) and (d) Plan and edge-on views of atomic relaxations around the vacancy. Each atomic relaxation is represented by a vector displacement projected on the plane of the paper.

Fig. 8 Displacement field around a vacancy in a [100] twist boundary (Σ=5, θ = 36.87°) in fcc copper. (a) and (b) Plan and edge-on views of relaxed structure before insertion of vacancy at encircled atom. (c) and (d) Plan and edge-on views of atomic relaxations around the vacancy. Each atomic relaxation is represented by a vector displacement projected on the plane of the paper.

Fig. 9 Displacement field around a vacancy in a [100] twist boundary (Σ=5, θ = 36.87°) in fcc nickel. (a) and (b) Plan and edge-on views of relaxed structure before insertion of vacancy at encircled atom.

(c) and (d) Plan and edge-on views of atomic relaxations around the vacancy. Each atomic relaxation is represented by a vector displacement projected on the plane of the paper.

Fig. 10 Same as Fig. 8 except that an in-plane translation of Lattice 1 with respect to Lattice 2 has not been imposed on the relaxed boundary structure, and the vacancy is in an O-Lattice site. O-Lattice sites indicated by X's.

Fig. 11 Same as Fig. 7(c) and (d) for tungsten except that the vacancy is in an O-Lattice site. O-Lattice points indicated by X's.

Fig. 12 Displacement field around a vacancy in a [100] symmetric tilt boundary (Σ=25, θ = 16.3°, boundary plane parallel to $(710)_{1,2}$) in bcc iron. (a) Edge-on view of relaxed structure before insertion of vacancy at the encircled atom. (b) Edge-on view of atomic relaxations around the vacancy. Each atomic relaxation is represented by a vector displacement projected on the plane of the paper.

Fig. 13 Displacement field around a vacancy in a [100] twist boundary (Σ=25, θ = 16.3°) in fcc copper. (a) and (b) Plan and edge-on views of relaxed structure before insertion of vacancy at encircled atom. (c) and (d) Plan and edge-on views of atomic relaxations around the vacancy. Each atomic relaxation is represented by a vector displacement projected on the plane of the paper. O-Lattice points indicated by X's.

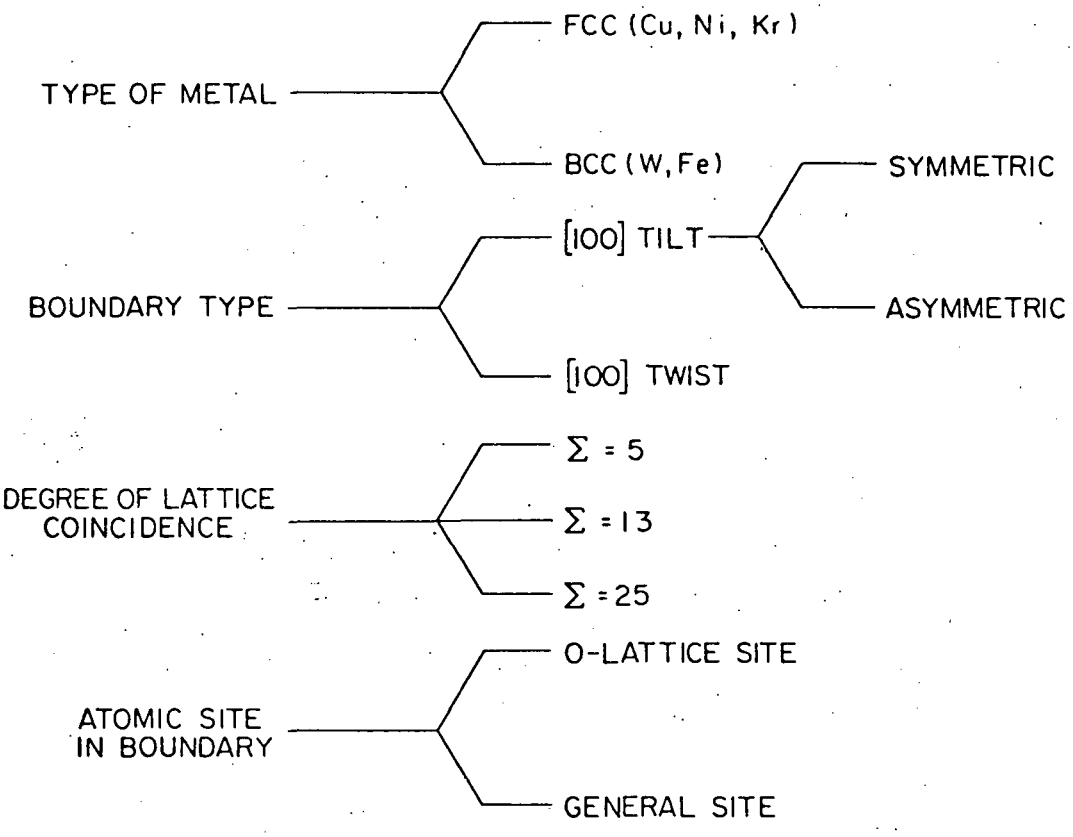
TYPE OF METAL
FCC (Cu, Ni, Kr)
BCC (W, Fe)
BOUNDARY TYPE
[100] TILT
SYMMETRIC
ASYMMETRIC
[100] TWIST
DEGREE OF LATTICE COINCIDENCE
Σ = 5
Σ = 13
Σ = 25
ATOMIC SITE IN BOUNDARY
O-LATTICE SITE
GENERAL SITE

FIG. 1

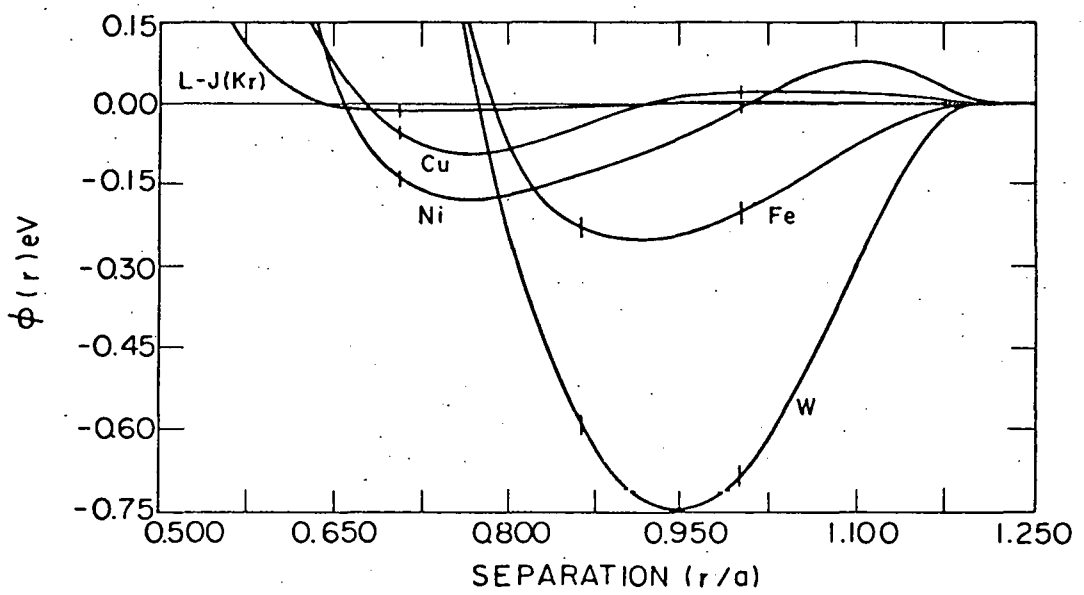
0.15
0.00
-0.15
-0.30
-0.45
-0.60
-0.75
φ(r) eV
L-J(Kr)
Cu
Ni
Fe
W
0.500
0.650
0.800
0.950
1.100
1.250
SEPARATION (r/a)

FIG. 2

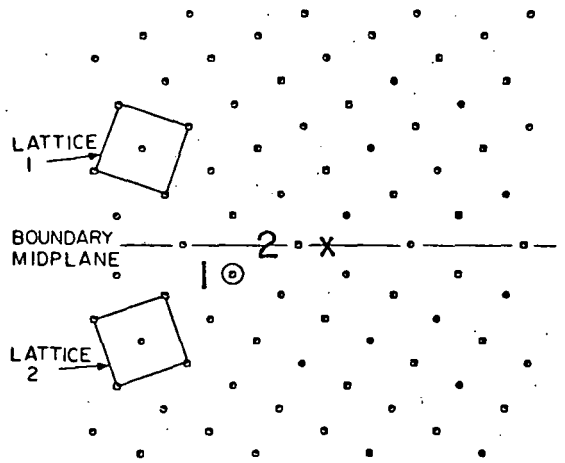

(a) VIEW EDGE ON

(b) VIEW EDGE ON

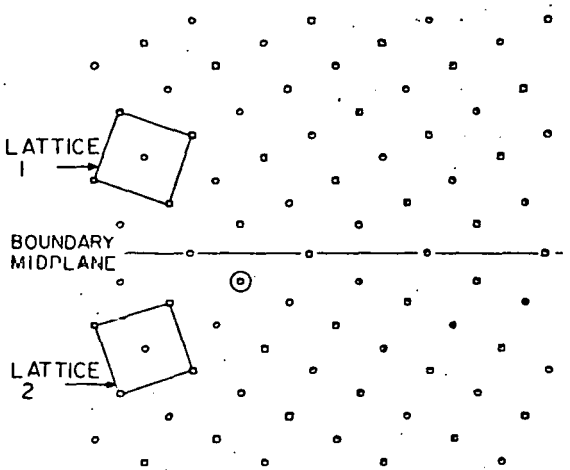

(c) VIEW EDGE ON

(d) VIEW EDGE ON

FIG. 3

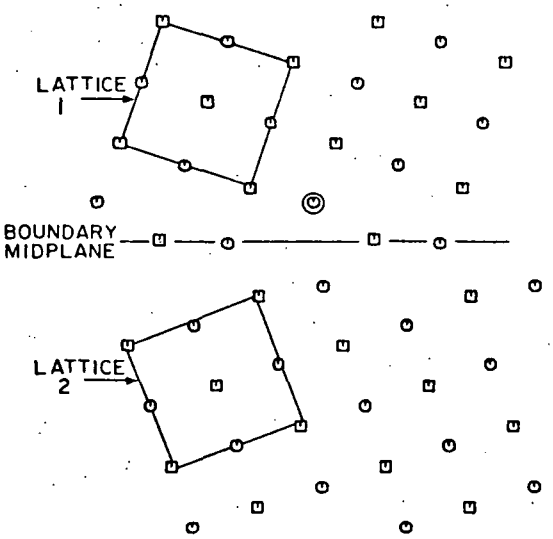

(a) VIEW EDGE ON

(b) VIEW EDGE ON

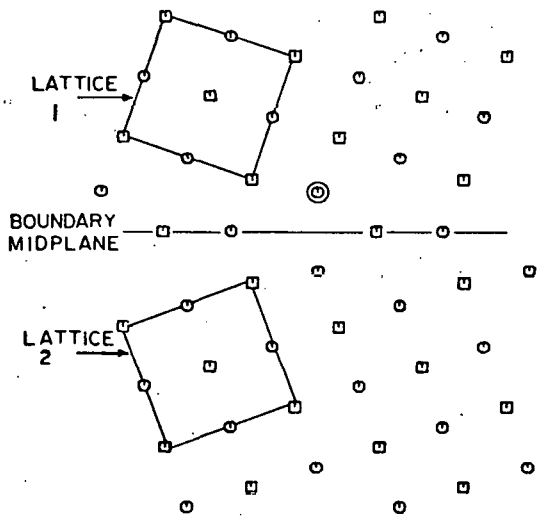

(c) VIEW EDGE ON

(d) VIEW EDGE ON

FIG. 4

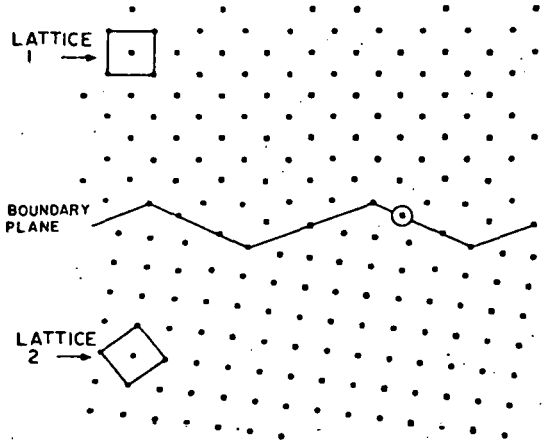

(a) VIEW EDGE ON

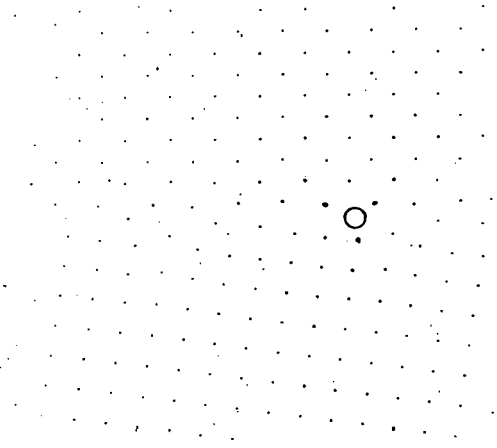

(b) VIEW EDGE ON

FIG. 5

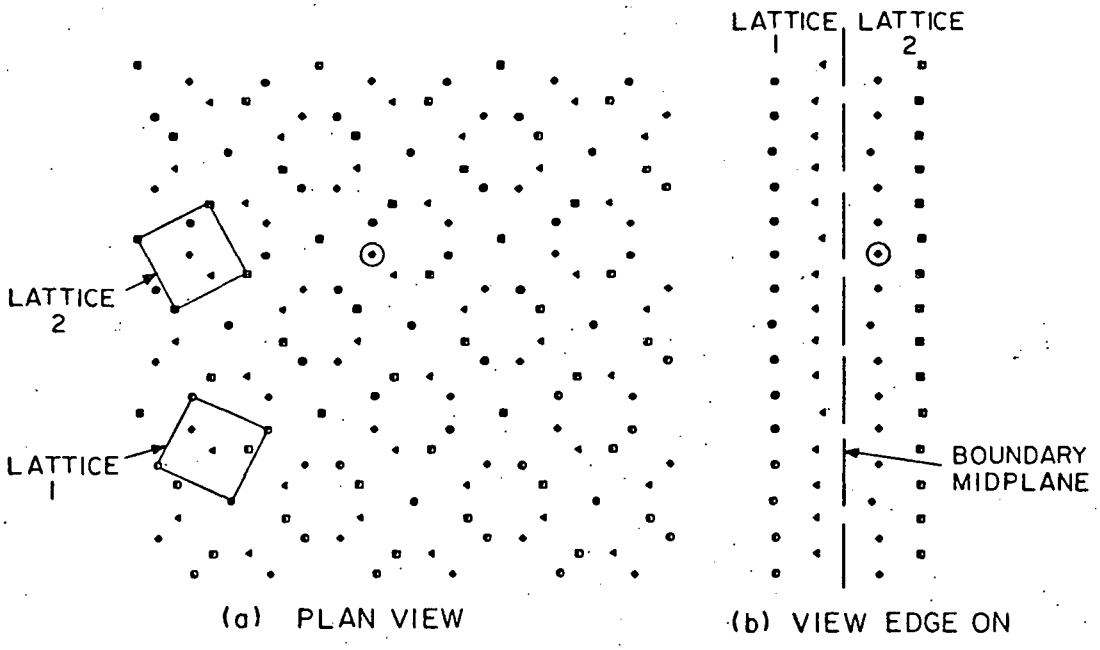

(a) PLAN VIEW

(b) VIEW EDGE ON

(c) PLAN VIEW

(d) VIEW EDGE ON

FIG. 6

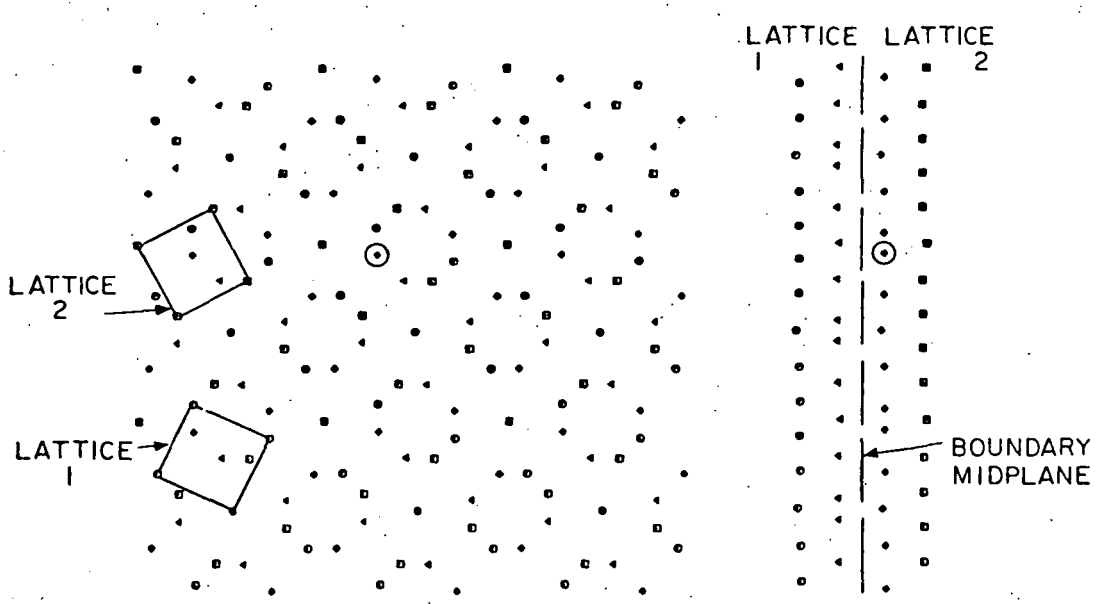

(a) PLAN VIEW

(b) VIEW EDGE ON

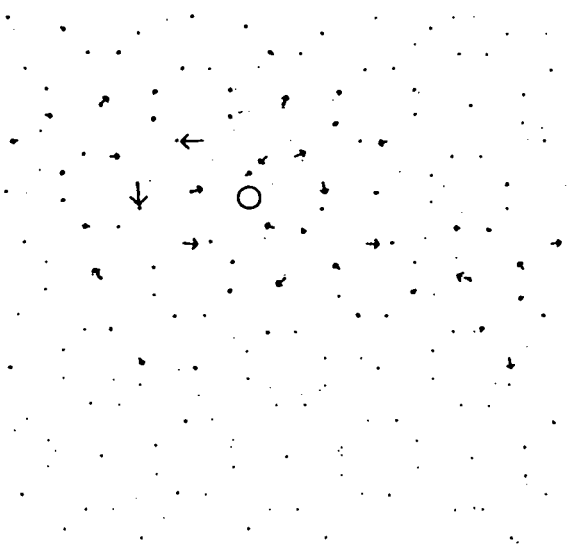

(c) PLAN VIEW

(d) VIEW EDGE ON

FIG. 7

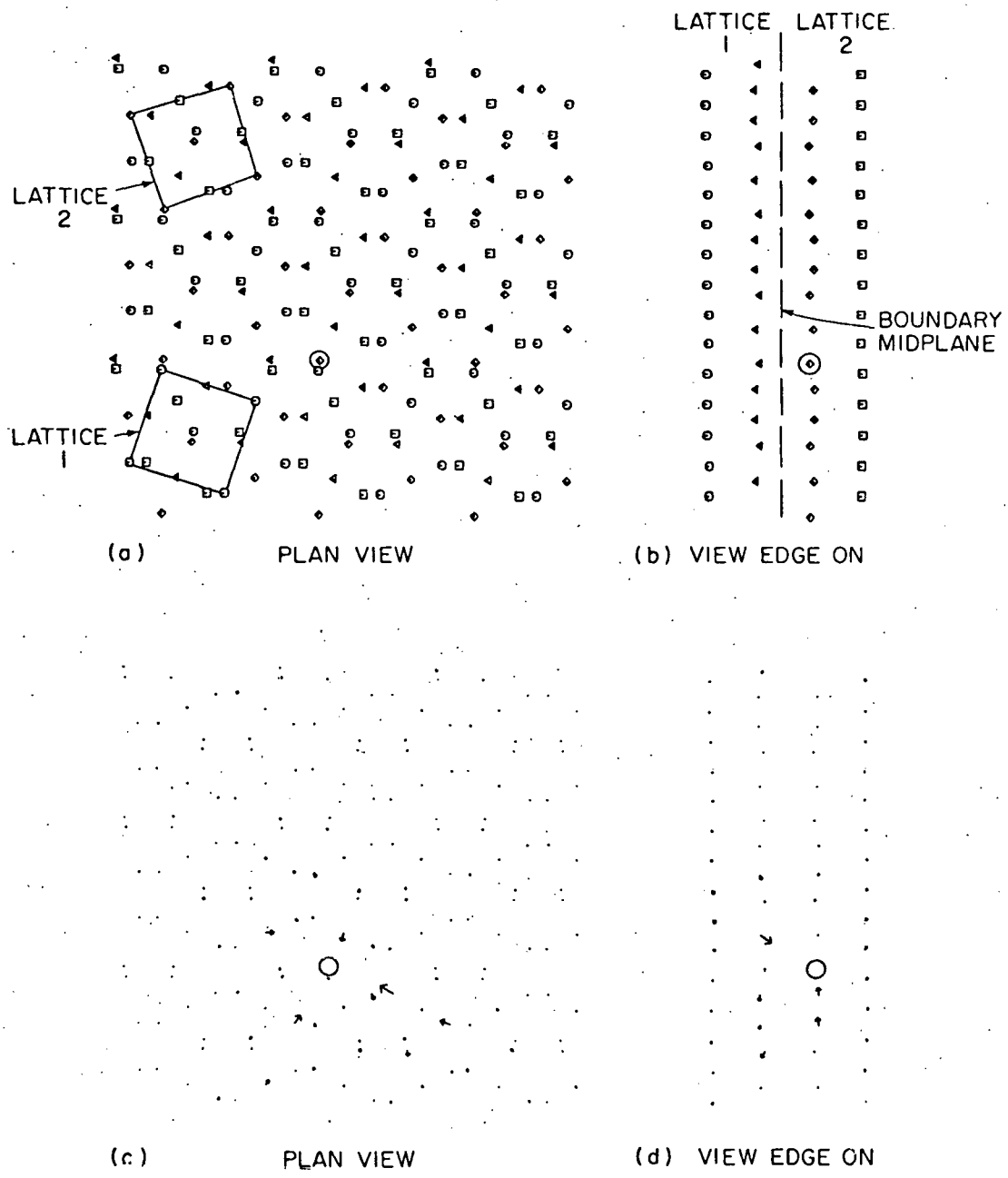
LATTICE 2
LATTICE 1
(a) PLAN VIEW
LATTICE 1
LATTICE 2
BOUNDARY MIDPLANE
(b) VIEW EDGE ON
(c) PLAN VIEW
(d) VIEW EDGE ON

FIG. 8

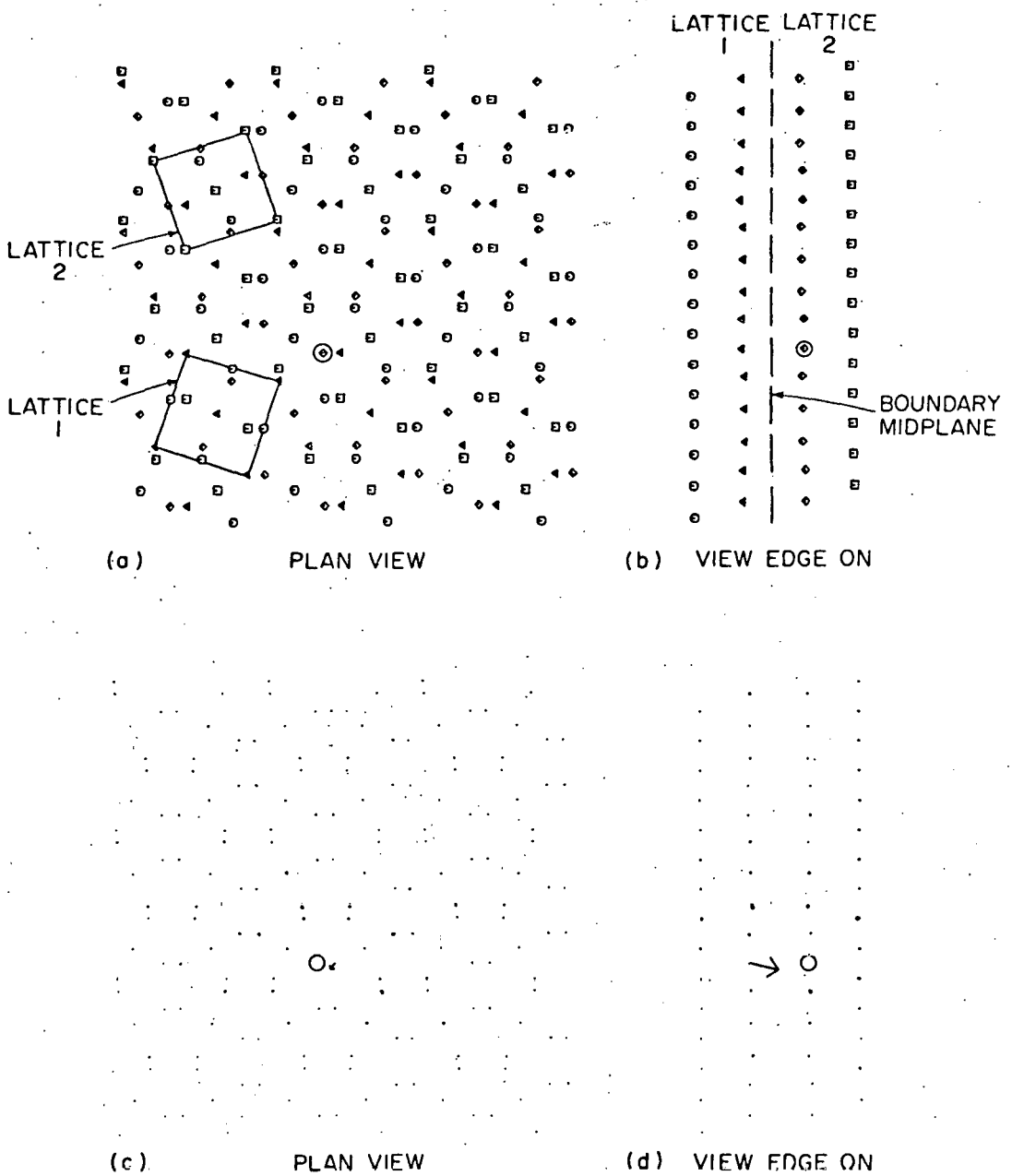
LATTICE 2
LATTICE 1
(a) PLAN VIEW
LATTICE 1
LATTICE 2
BOUNDARY MIDPLANE
(b) VIEW EDGE ON
O
(c) PLAN VIEW
O
(d) VIEW EDGE ON

FIG. 9

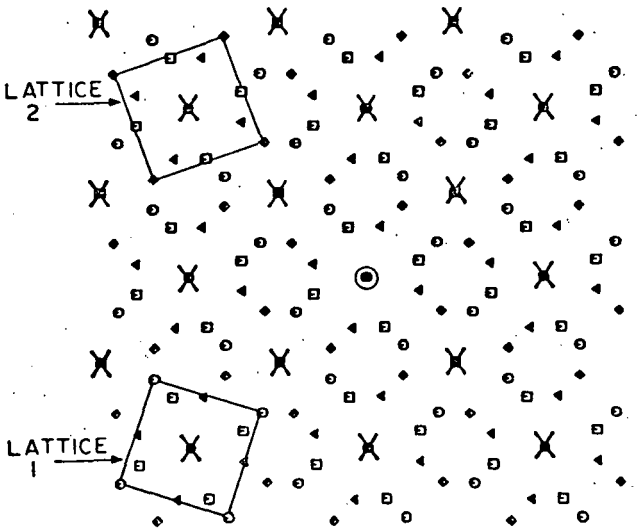

(a) PLAN VIEW

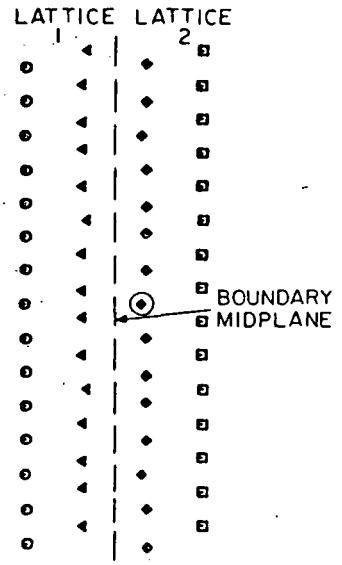

(b) VIEW EDGE ON

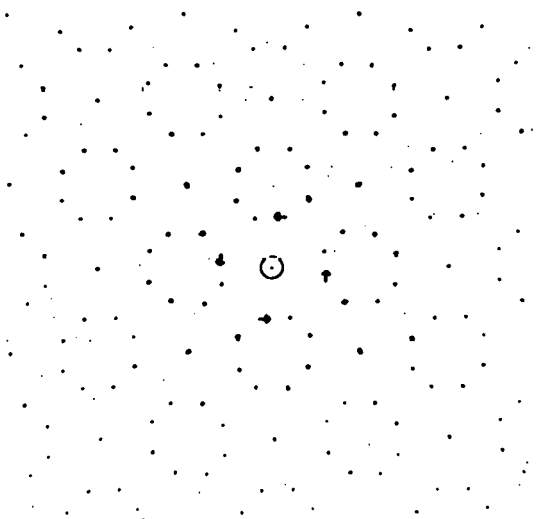

(c) PLAN VIEW

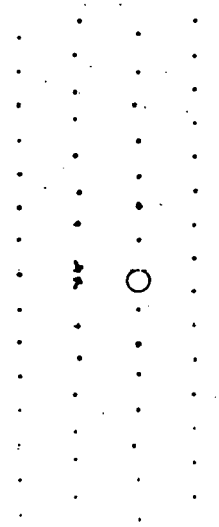

(d) VIEW EDGE ON

FIG. 10

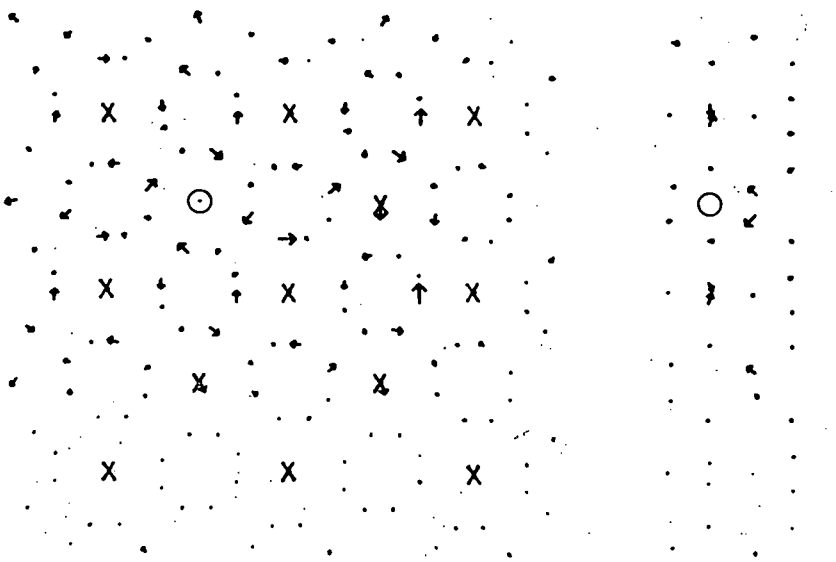

(a) PLAN VIEW (b) VIEW EDGE ON

FIG.11

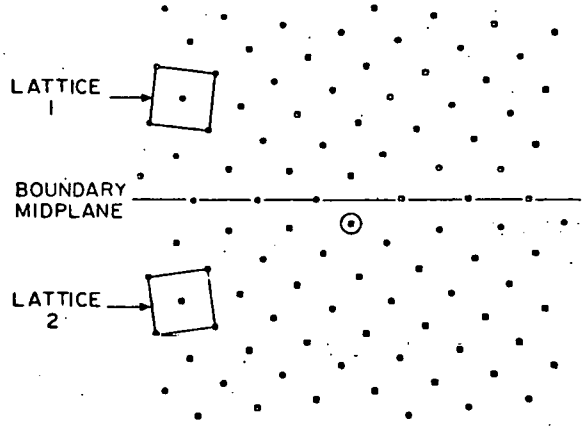

(a) VIEW EDGE ON

(b) VIEW EDGE ON

FIG. 12

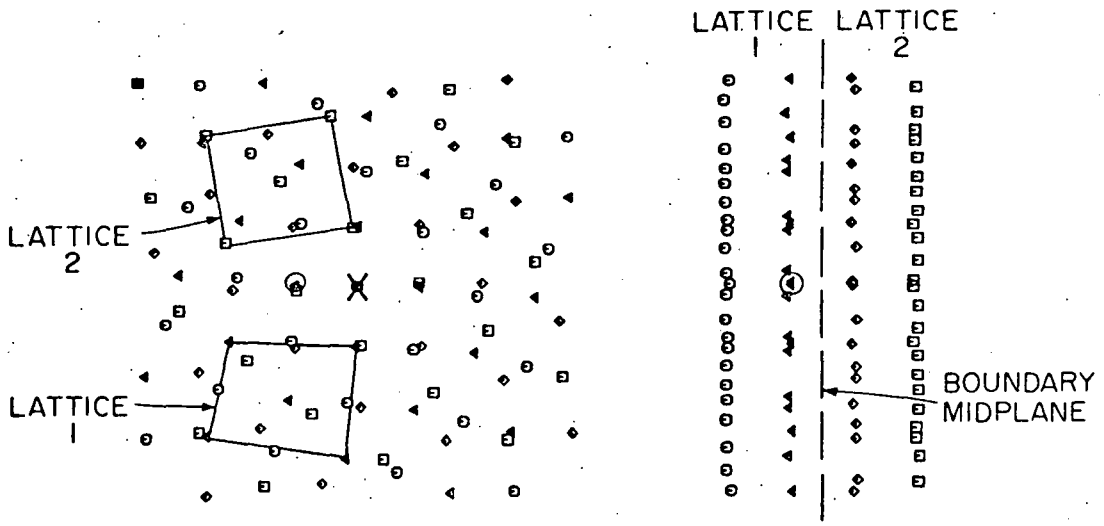

(a) PLAN VIEW (b) VIEW EDGE ON

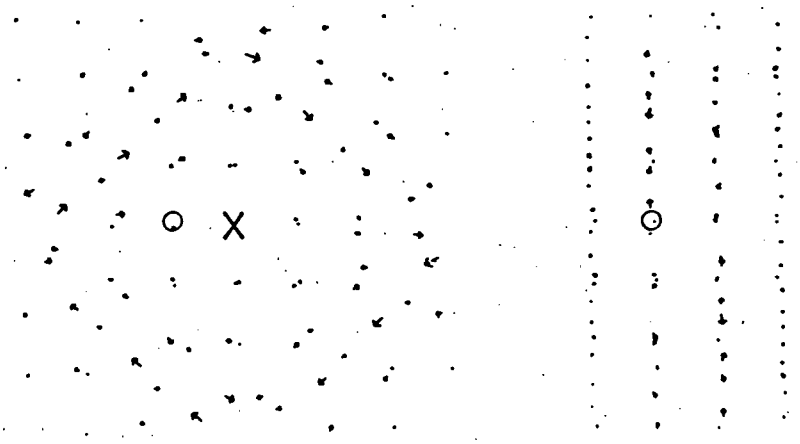

(c) PLAN VIEW (d) VIEW EDGE ON

FIG. 13